X-ray spectroscopy and local structures in glasses†

K J RAO* and B G RAO

Solid State and Structural Chemistry Unit, Indian Institute of Science, Bangalore 560012, India

Abstract. X-ray spectroscopy which is a combination of two techniques, namely x-ray absorption near edge structure (XANES) and extended x-ray absorption fine structure (EXAFS) analyses, is a unique technique for the study of local structures in glasses. Availability of synchrotron radiation sources has made the technique quite attractive and useful because the photon flux from synchrotrons is very intense and polarized. In this article, a brief summary of XANES and EXAFS techniques is given along with a few applications to the study of local structures in glasses.

Keywords. X-ray spectroscopy; XANES; EXAFS; photon flux; synchrotron radiation.

1. Introduction

Among the new tools that have become available for the investigation of the structure of disordered solids, x-ray spectroscopy is unique (Azaroff 1977; Winick and Donaich 1980). It is in reality a combination of two techniques, namely analyses of x-ray absorption near edge structure (XANES) and extended x-ray absorption fine structure (EXAFS). Its uniqueness ensues from the fact that absorption edges are atom specific. Therefore it enables one to analyze the fine structures associated with the x-ray absorption edge of any particular atom and obtain information about the surrounding structure. Further, as we shall see later, the EXAFS arises largely from the scattering effect of the nearest neighbours in the structure (Lytle 1965; Sayers et al 1971). Therefore the information contained in EXAFS is largely about the local structures.

Several aspects of x-ray spectroscopy have been known for a long time (Azaroff 1963). But it was not until 1971 that the so-called Kronig structure in x-ray spectra of materials which is now known as EXAFS was shown to arise from short range order by Sayers et al (1971). They demonstrated through Fourier transform techniques that structural information can be evaluated quantitatively from EXAFS. The last decade has seen a very large number of applications of EXAFS technique in the analysis of local structures in glasses, catalysts, biological samples and a host of crystalline and non-crystalline materials with great benefit. A large number of reviews and monographs have appeared on this technique (Stern 1978; Hayes 1978; Lee et al 1981; Wong 1981; Teo and Joy 1981; Hayes and Boyce 1982; Parthasarathy et al 1982). The theoretical situation with XANES, on the other hand, is not as well developed as that of EXAFS. This is natural because chemical effects and symmetry of the surrounding atoms affect the region around edge absorption upto a few eV which arise due to excitation to bound states. In this region XANES can be analyzed within the framework of spectroscopy (Best

---

* To whom all correspondence should be addressed.

1966; Shulman et al 1976; Tsutsumi et al 1977; Grunes 1983; Rao and Wong 1984; Rao et al 1985b). Symmetry information resulting from xanes analysis can be combined with the structural information derived from exafs. Together exafs and xanes can therefore provide a very powerful tool for investigation of local structure (Rao et al 1983, 1984a, 1985c). Since the advent of synchrotron radiation sources x-ray spectroscopy has become a popular and powerful method particularly for the investigation of glasses. In this article an attempt has been made to provide a brief outline of the exafs and xanes procedures and discuss the strengths and weaknesses of these techniques in the structural elucidation of glasses with illustrative examples from the authors' work.

2. Principles of the EXAFS and the XANES

When sufficiently energetic x-ray photons are incident on solids, electrons from the core levels are excited. This gives rise to an absorption edge. At photon energies greater than the edge energy, absorption coefficients decay and the decaying profile in solids, liquids and complex molecules are characterized by intensity modulations. The strength of these modulations themselves ultimately decay at higher photon energies. A typical edge absorption spectrum is shown in figure 1a. The region of spectra upto about 30 eV above the edge is generally considered as xanes while undulations above 40–50 eV constitutes the exafs region. The normalized near edge structure (xanes) obtained from the edge spectrum (given in figure 1a) is shown in figure 1b. In the region of the near edge the interaction of the photoelectron with the atom is very strong. In fact, closer to the edge the photoelectron explores allowed final states only and hence the near edge has all the features of a normal core electron excitation spectrum. However, the allowed energy states of the atom get compressed into a Rydberg continuum and it is also
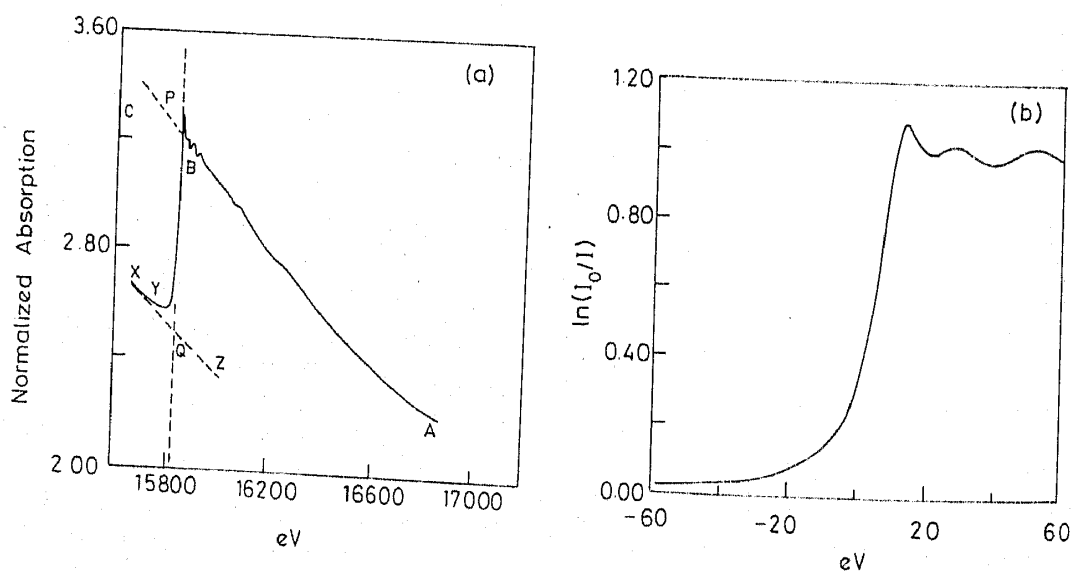

Figure 1. (a) Room temperature Pb L_1 absorption spectrum of lead foil, schematically showing the edge normalization procedure (see Rao et al 1985b); (b) Normalized edge spectrum in the range ±60 eV. The zero of energy is taken with respect to the L_1 edge of Pb at 15860·8 eV.

possible that the spatial extension of such states gives rise to formation of energy bands. When the energy of the electron is of the order of 40 to 50 eV it essentially behaves like a free electron propagating into the solid and scattered as in low energy electron diffraction. The variation of low energy electron diffraction condition as a function of energy causes the EXAFS undulations.

The propagation of the photoelectron may be approximated to a spherical wave spreading outwards from the atom as shown in figure 2. A fraction of the spherical wave is reflected back from the surrounding atoms which interferes with the outgoing wave. Due to this interference both the amplitude and the phase of the electron wave at the origin is affected. The absorption coefficient, μ, which is proportional to the dipole-transition matrix element (Eisenberger and Kincaid 1978) is therefore affected by the scattered part of the wave function, ψ_{sc}.

$$\mu(h\nu) \propto |\langle \psi_i | r | \psi_f + \psi_{sc} \rangle|^2 \qquad (1)$$

It is easy to visualize that at very large k values the amplitude of the scattered wave decreases with the increasing wave vector of the electron because higher the energy of the electron weaker is the scattering amplitude from the surrounding atoms. The phase, however, being a periodic function gives rise to oscillatory behaviour of ψ_{sc} and hence of μ which is the origin of EXAFS. The theory of EXAFS has been worked out in the single electron approximation assuming the propagating electron wave to be planer. The EXAFS, χ, as is to be expected, is determined by the combined effect of scattering from various shells of neighbours which in a crystal are situated at specific distances. Further the intensity of the propagating wave itself decreases as the square of the distance of the scatterer. It has been shown (Sayers *et al* 1971) that

$$\chi(k) = -\frac{1}{k} \sum_j A_j \sin\left[2r_j k + \phi_j(k)\right], \qquad (2)$$

where,

$$A_j = (N_j/r_j^2)|f_j(\pi, k)| \exp(-2r_j/\lambda) \exp(-2\sigma_j^2 k^2), \qquad (3)$$

where k is the wave vector of the propagating electron wave and k is given by $(1/\hbar)$ $[2m(h\nu - E_b)]^{1/2}$ where E_b is the binding energy of the core electron. N_j is the number of neighbours in the jth shell which is at a distance r_j; $f_j(\pi, k)$ is the complex amplitude
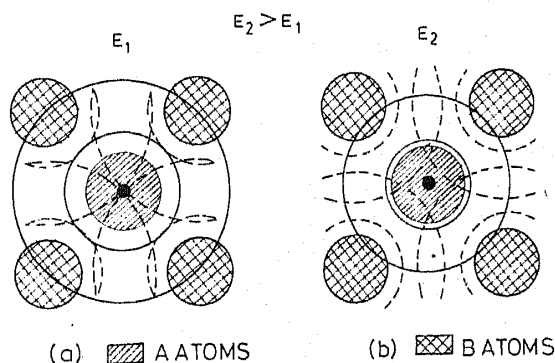

Figure 2. A schematic representation of the EXAFS process; the solid circles denote outgoing waves centred about absorber atoms A and broken circles denote reflected waves centred about scatter atoms B. Constructive interference is depicted in (**a**) and destructive interference in (**b**).

of scattering wave; ϕ_j is the phase shift; σ_j is the Debye-Waller factor for EXAFS which produces a spread in r_j and hence a loss of EXAFS amplitude and λ is the electron mean free path which is generally so high that the exponential term containing λ does not affect the observed χ. In the above expressions while the sinusoidal phase term produces the oscillatory behaviour, the envelope of χ arising from a given shell is determined primarily by the behaviour of $f_j(\pi, k)$ (σ_j is generally low at very low temperatures).

Thus the EXAFS function contains the three structural parameters, r_j, N_j and σ_j and three scattering parameters, ϕ_j, f_j and λ (Wong 1981). $\chi(k)$ can be Fourier transformed to yield structure functions in r space which is essentially a pair distribution function containing relevant structural information. However, it requires one to know ϕ_j, f_j and λ in order to calculate r_j, N_j and σ_j (Stern *et al* 1975).

3. Experimental method

A schematic of x-ray spectroscopy experimental set up at a synchrotron facility is shown in figure 3. Monochromatization of the x-rays from the synchrotron is achieved by double reflection from parallelly placed (220) cut Si crystals, the movement of one of the Si plates is accomplished through a weak-link. The intensities are detected using photo-ionization chambers. Photon counting procedures employ proportional counters and are used when measurements are done in fluorescence mode. Higher excitation voltages are needed in the study of K and L edges of heavy elements. Convenient intensities at such energies are available in synchrotron facilities whose operating voltages are very high such as at Cornell high energy synchrotron source (CHESS) facility operating at ~ 5 GeV. The radiation from synchrotron sources usually range from 10^{12} to 10^{13} photons per milliradian per m amp per 10% band width and is highly polarized.

4. Data analysis

In actual practice the edge spectrum of an atom in a sample is obtained by passing an x-ray beam of intensity I_0 through the sample and recording the intensity I of the transmitted beam. The quantity $\ln(I_0/I)$ is directly proportional to the absorption coefficient, μ. A typical raw spectra is plotted in figure 4a as $\ln(I_0/I)$ vs. $(E - E_b)$ where E is the energy of the x-ray beam. In the next step the quantity $(E - E_b)$ is converted to k
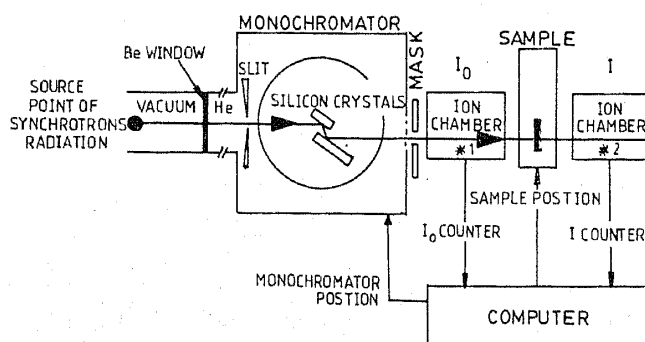

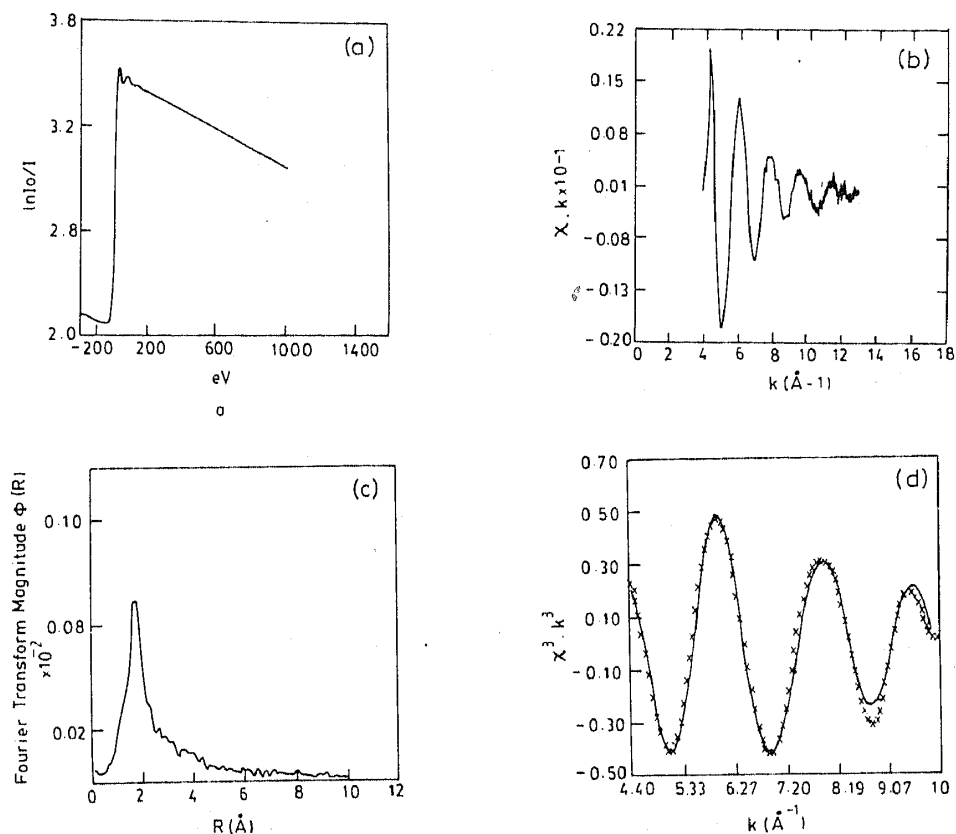Figure 3. A schematic diagram of a typical EXAFS experimental set-up.

Figure 4. The steps in the analyses of EXAFS is shown for a typical 80PbO.20PbCl$_2$ glass: (a) raw spectra of the L_3 edge of Pb; (b) normalized EXAFS; (c) radial structure function $\Phi(r)$; (d) inverse Fourier transform (solid line) and simulated EXAFS (crosses) of the first peak in $\Phi(r)$ from (c).

using the formula given earlier and the EXAFS, $\chi(k)$ is computed as a function of k by the following formula,

$$\chi(k) = \frac{\mu(k) - \mu_0(k)}{\mu_0(k)\, M(k)} \qquad (4)$$

where μ_0 is the smoothly decaying (atomic) background absorption and $M(k)$ is the McMaster correction. The plot of $\chi(k) \cdot k$ vs k is given in figure 4b. Generally either due to large values of σ_j or inherently weak $\chi(k)$, which is due to the rapidly diminishing $f_j(\pi, k)$ particularly for low atomic weight first neighbours, $\chi(k)$ diminishes very rapidly with k and it is required to accentuate this region by weighting the $\chi(k)$ values with k^n. The product $\chi(k) \cdot k^n$ is then Fourier transformed in finite k space (between k_{min} and k_{max}) to obtain the radial structure function $\Phi^n(r)$, which is given as

$$\Phi^n(r) = \left(\frac{1}{2\pi}\right)^{1/2} \int_{k_{min}}^{k_{max}} k^n \cdot \chi(k) \exp\left[2ikr\right] dk, \qquad (5)$$

where $W(k)$ is a window function. $\Phi^n(r)$ is characterized by a number of peaks at various r_j values (figure 4c). However, these r_j values are generally smaller than the actual distances due to the k-dependence of the phase shift, ϕ_j, which is not taken care of in the Fourier transform. Nevertheless, computation of $\Phi^n(r)$ constitutes the first major step

in the analysis of EXAFS because the separated peaks in r-space enable the separation of the χ_j contribution from various shells. The first peak in $\Phi''(r)$ which is denoted as $\Phi''(r_1)$ arises from the Fourier transformation of $k^n.\chi_1(k)$. Hence $\Phi''(r_1)$ can be inverse Fourier transformed to recover $k^n.\chi_1(k)$. The structural parameters N_j, r_j and σ_j can be obtained from the isolated $k^n.\chi_j(k)$ by two procedures. In both procedures, it is necessary to perform a similar EXAFS analysis of a model sample of known structure which has a close chemical similarity with the sample of unknown structure.

The first procedure is relatively simple. If $\chi_1^U(k)$ and $\chi_1^M(k)$ corresponding to the unknown and the model are computed from their EXAFS data, then a plot of $\ln[\chi_1^U(k)/\chi_1^M(k)]$ vs k^2 will enable the determination of the coordination number, N, and the Debye-Waller factor, σ of the unknown sample (Stern *et al* 1975; Elliott 1984). The r-shifts observed with the model sample can then be used to obtain the r value of the unknown sample. In the second procedure which is more accurate and popular, $\chi_1^M(k)$ is first curve-fitted using the known structural parameters in order to obtain the best-fit scattering parameters. In doing so tabulated theoretical values of $f_j(\pi, k)$ and $\phi_j(k)$ relevant for the emitter-scatterer pairs from the work of Teo and Lee (1979) and null values of σ_j are used as initial sets in the iterative optimization of scattering parameters. The optimization is done by non-linear least-square fitting methods. Generally the phase shift, $\phi(k)$ is expressed as a polynomial of the form (Lee *et al* 1977)

$$\phi(k) = p_0 + p_1 k + p_2 k^2 + p_3/k^3 \tag{6}$$

The values of p_0, p_1, p_2 and p_3 are determined from curve fitting. The scattering parameters obtained from curve-fitting the EXAFS data of the model are assumed to be transferable and then curve-fitting of $\chi_1^U(k)$ is performed with the new input scattering parameters to obtain the optimized values of the structure parameters of the unknown. The curve fitting of $\chi_1^U(k)$ is shown in figure 4d.

The EXAFS analysis provides sufficiently direct information about both the distances and the numbers of neighbours in various shells, particularly in the first shell. But the geometrical arrangement of N neighbours around the central atom at a distance r (or at further distances) is not easy to obtain from EXAFS alone without further assumptions. When the first shell of neighbours conforms to a simple geometrical shape, XANES can be effectively exploited to fix the spatial configuration. This is particularly attractive when L edge spectra are studied. It may be noted here that the final states for L_1 edge are vacant p states and for L_2 and L_3 edges the final states are d states. These final states are split by the local crystal fields and hence the absorption peaks are also split correspondingly. The nature of splitting observed in XANES and the value of coordination number obtained from EXAFS analysis can often be easily combined to guess the right geometry of the nearest neighbour polyhedron.

In order to be able to use EXAFS effectively in the analysis of local structure in glasses one has to take note of the fact that the coordination polyhedra around an atom in a glass is distorted more as a rule than as an exception. Hence there is a distribution of r_j values even in the first shell itself. It has therefore been found profitable to treat the first neighbours as being present in subshells and extend the fitting procedures indicated earlier with appropriately large number of structural parameters. It is also necessary to analyse the EXAFS of the model with the same number of sets of phase parameters (Wong and Liberman 1984; Rao *et al* 1984b).

Let us now consider a few typical examples of EXAFS and XANES application to structural studies of glasses.

5. Case studies

5.1 *Coordination of Pb in lead oxyhalide glasses*

In an attempt to examine the coordination of Pb in lead oxyhalide ($PbO-PbF_2$ and $PbO-PbCl_2$) glasses, EXAFS associated with Pb L_3 edge was investigated (Rao *et al* 1984b). The method of analysis described earlier was used. The raw spectra, the normalized EXAFS and radial structure function $\Phi(r)$ for a typical $PbO-PbCl_2$ glass are given in figures 4a, b and c respectively. The radial peak around 2·0 Å was inverse Fourier transformed to obtain $\chi(k)$ contribution from the first shell (figure 4d). The scattering parameters required for curve-fitting were obtained from the analysis of the EXAFS of Pb in crystalline PbO and $PbCl_2$. The resulting phase parameters are given in table 1 along with the input crystal data. These phase parameters have been used to fit the $\chi(k)$ of glasses and the structural parameters for various $PbO-PbCl_2$ glasses were obtained. The structural parameters for a typical glass are given in table 2 and the spectrum simulated in the curve fitting procedure is also shown in figure 4d. It may be noted from table 2 that the total N_j values for the glass is close to 6·0 within $\pm 5\%$. Almost similar values of N_j were obtained for all other glass compositions. EXAFS studies of $PbO-PbCl_2$ glasses have thus enabled to establish the presence of

Table 1. Input crystal data and computer fitted values of Pb–O and Pb–Cl phase shift parameters for PbO and $PbCl_2$ crystals from the respective Pb–L_3 edge EXAFS

Compound	r_j	n_j	σ^2 ($A^2 \times 10^2$)	p_0	p_1	p_2	p_3	Standard deviation of fit (% of max value)
PbO	2·215	2	0·983	5·1472	−1·0823	0·0247	51·80	
(yellow)	2·490	2	1·016	5·2403	−1·1384	0·0161	143·88	6·8
	2·670	2	3·077	0·1557	−1·4191	0·0522	21·16	
	2·880	1	18·873	5·9105	−1·5667	0·0487	16·18	
$PbCl_2$	3·065	2	3·531	5·6566	−1·5328	0·0328	33·26	7·4
	3·130	2	3·367	0·4443	−1·4950	0·0133	30·71	
	3·290	2	3·427	0·4173	−1·4815	0·0077	29·45	

Table 2. Structural parameters for a $PbO-PbCl_2$ glass obtained from the analysis of L_3 edge EXAFS spectra of Pb

Composition $PbO:PbCl_2$	Coordinating atom in the shell	r_j (A)	N_j	σ^2 ($A^2 \times 10^2$)	ΣN_j	Standard deviation of fit (% of max value)
	O	2·21	1·04	0·283		
	O	2·46	1·07	0·116		
8:20	Cl	2·70	0·80	0·190		
	Cl	2·72	0·83	1·513	6·26	7·5
	Cl	3·04	0·92	0·307		
	Cl	3·10	1·00	0·204		
	Cl	3·29	0·62	0·330		

$[PbO_2Cl_4]$ groups, which confirmed an earlier postulate from the x-ray diffraction study (Rao and Rao 1984). XANES analysis also indicated the presence of $[PbO_2Cl_4]$ groups (Rao and Wong 1984). EXAFS of $PbO-PbF_2$ glasses have been analysed similarly (Rao *et al* 1985a) along with the detailed analysis of the near edge structure (Rao *et al* 1985b). It has been shown that while EXAFS reveals the presence of $[PbO_2F_4]$ units throughout the glass forming composition, XANES suggests that the symmetry of these units gradually evolves from $C_s \rightarrow C_{2v} \rightarrow D_{4h} \rightarrow O_h$ as PbF_2 content increases in the glass.

5.2 *Coordination of Nd in NdF_3-BeF_2 glasses*

Another example of structural application of EXAFS is the investigation of Nd coordination in NdF_3-BeF_2 glasses. Previous computer simulation studies of these glasses have indicated Nd coordination smaller than in NdF_3. For this purpose EXAFS and XANES of L_3 and L_2 edges of Nd^{3+} have been investigated (Rao *et al* 1983). The near edge features of Nd^{3+} in BeF_2 glasses is similar to that in Nd_2O_3 rather than in NdF_3 (figure 5) suggesting that Nd coordination in glasses is similar to that in Nd_2O_3, which is equal to seven. In order to determine the local structure around Nd in the glass from EXAFS phase parameters for Nd–F pairs were obtained from EXAFS analysis of crystalline NdF_3. The inverse Fourier transforms obtained from the analysis of the EXAFS associated with L_2 and L_3 edges of the glass were curve-fitted with a four shell simulation involving eleven F^- ions. The final values of structural parameters obtained in this fit are given in table 3.

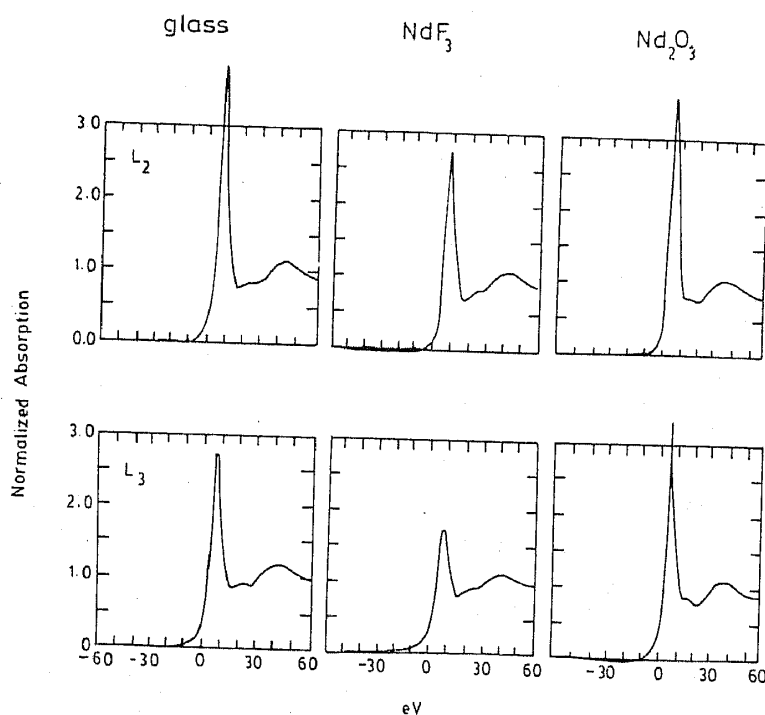It is noteworthy that the distances obtained from EXAFS analysis of both L_3 and L_2

Figure 5. Normalized XANES scans for NdF_3-BeF_2 glass, crystalline NdF_3 and Nd_2O_3 at the L_2 and L_3 edges. Zeros for the energy scale are taken at the corresponding edge energies of Nd metal at $L_2 = 6721 \cdot 5$ eV and $L_3 = 6208$ eV.

Table 3. Structural parameters obtained from EXAFS for the NdF$_3$–BeF$_2$ glass

r_j (A)	N_j	ΣN_j	σ ($\pm$A)	Standard deviation of fit (% of max. value)
L$_2$ edge				
2·33(5)	1·52 ⎫		0·0761	
2·42(6)	3·35 ⎬ 7·14		0·1011	
2·52(7)	2·27 ⎭		0·0848	7·5
3·04(5)	2·13		0·1350	
L$_3$ edge				
2·35(5)	1·71 ⎫		0·0722	
2·45(5)	2·67 ⎬ 7·07		0·1352	
2·60(8)	2·69 ⎭		0·1169	9·1%
3·05(1)	1·14		0·1273	

Table 4. Structural parameters from EXAFS analysis of L_3 edge of 0·33 ThF$_4$ · 0·60 HfF$_4$ · 0·07 LaF$_3$ glass

N (A)	r (A)	σ^2 (A^2)	Standard deviation of EXAFS fit
2·89	1·83	0·0092	
3·17	1·92	0·0065	7%
2·07	1·99	0·0005	

edges are internally consistent. The numbers of nearest neighbours agree with the L_3 and L_2 edge analysis to within 12%. If we consider the fourth shell neighbours which are at a distance of 3·05 Å in the glass as non-nearest coordination, then the nearest neighbour coordination is from the first three shells to a radius of 2·60 Å and the total number of neighbours add upto ~ 7 which is the same number inferred from the similarly of XANES of the glass and Nd$_2$O$_3$.

5.3 Coordination of Th in a ThF$_4$–HfF$_4$–LaF$_3$ glass

In a similar investigation of the EXAFS of Th^{4+} in crystalline ThF$_4$ and ThF$_4$–HfF$_4$–LaF$_3$ glass, it was shown that the coordination number of Th^{4+} ion is the same (four) in both crystalline and amorphous state (Rao *et al* 1984a). The structural parameters obtained by EXAFS analysis for crystalline ThF$_4$ and the glass are given in table 4. It may be noted that the Th–F distances in the glass are very nearly equal (within 0·01 Å) to those in crystalline ThF$_4$. The lower σ_j^2 values of the two innermost subshells are also of interest in comparison to those of the crystals. This may be reflective of a covalency effect due to glass formation. In fact the white line intensity of the Th L_3 edge is about 12% higher in the glass than in crystalline ThF$_4$ (figure 6) suggesting that Th is more covalently bonded in the glass.
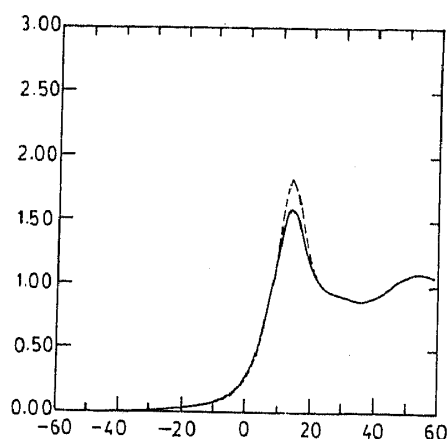
Figure 6. Normalized XANES of Th L_3 edge for crystalline ThF_4 (solid line) and $33ThF_4.60HfF_4.7LaF_3$ glass (dashed line). The zero of the energy scale is taken at the L_3 edge energy of Th metal at 16300 eV.

5.4 *Coordination of Mo in $AgI-Ag_2O-MoO_3$ glasses*

In view of a pronounced tendency of Mo for octahedral coordination in oxides, we thought it interesting to investigate MoO_3 containing glasses. Infrared spectroscopic studies of $AgI-Ag_2O-MoO_3$ glasses indicated the presence of tetrahedral MoO_4^{2-} ions with a possibility of distortion of its tetrahedral (T_d) symmetry (Hemlata *et al* 1983). To investigate this, XANES and EXAFS associated with the Mo K-edge in the glasses were investigated (Rao *et al* 1985c). The XANES spectrum of the glass was found to be similar to that of Na_2MoO_4 and different from that of MoO_3 (figure 7) indicating that Mo coordination in the glass is tetrahedral as in Na_2MoO_4 and not octahedral as in MoO_3. Further, EXAFS analysis of glasses with a single-shell simulation gives a coordination of four for Mo atoms in the glasses (see table 5). However, the second peak in the differentiated spectra of the glass (see the inset to figure 7c) appears to be split indicating a possible distortion of the MoO_4^{2-} tetrahedra. A molecular orbital analysis (figure 8) suggests that the second peak arises from a transition from 1s atomic level of molybdenum to 2t m.o. levels. A distortion of MoO_4^{2-} unit causes the splitting of 2t level which is responsible for the splitting of the second peak. In order to investigate these possible distortions which give rise to different Mo–O distances the EXAFS of these glasses were re-analysed assuming that there are two oxygens each at two different distances. The results of two-shell analysis of EXAFS are also given in table 5. The two-shell fit gives a coordination number much closer to four and a bond distance which is slightly longer (1·92 Å) than the other three bond distances (1·83 Å). It should be noted that the standard deviations for both single-shell and two-shell simulations are very similar. This brings out one of the weaknesses of EXAFS analysis. This weakness of the EXAFS technique may probably be due to the multiparametric nature of phase-shift evaluation.

6. Limitations of EXAFS and XANES methods

One of the important limitations of the EXAFS technique arises from the assumption that phases and amplitudes are transferable. Two other somewhat serious limitations are (i) inadequate correction for multiple and inelastic electron scattering effects and (ii) uncertain scaling of k due to choice of E_b.
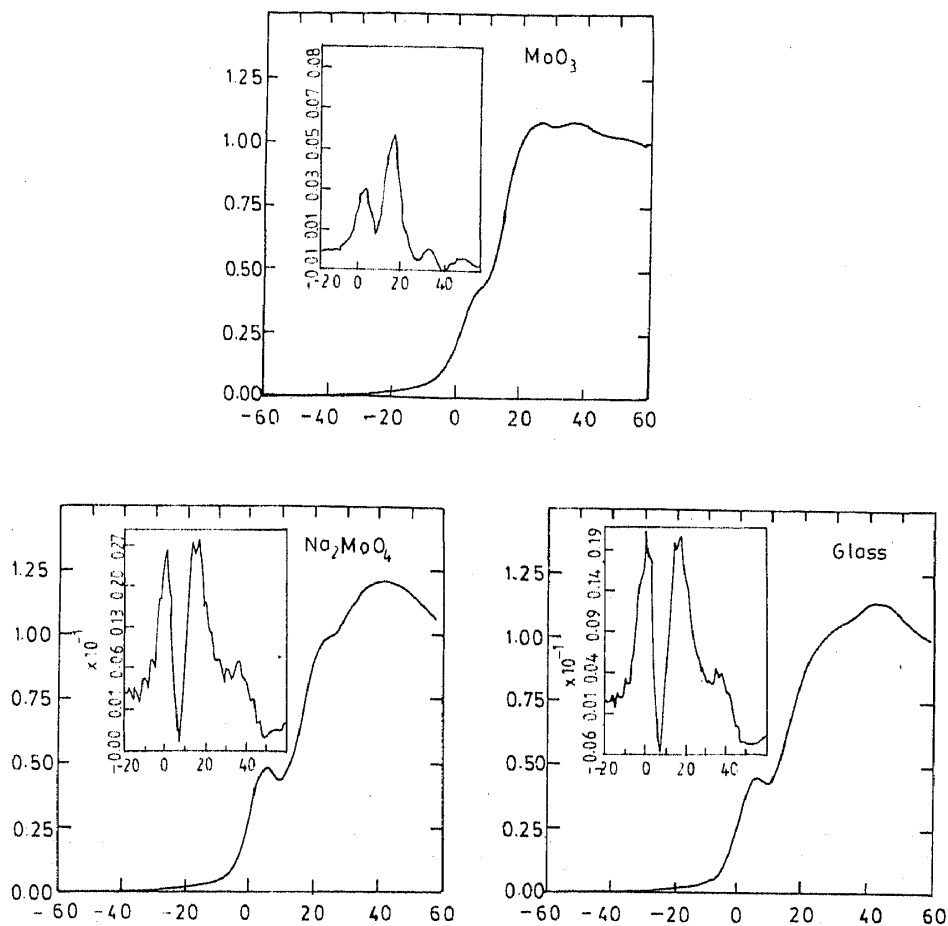
Figure 7. Normalized XANES of Mo K edge in MoO_3, Na_2MoO_4 and $40AgI-30Ag_2O-30MoO_3$ glass. The differentiated spectra are given in the inset.

Table 5. Structural parameters from EXAFS analysis of $AgI.Ag_2O.MoO_3$ glasses

Glass composition $AgI:Ag_2O:MoO_3$	N	r (Å)	σ^2 (Å^2) $\times 10^2$	Standard deviation %
A. One shell				
60:20:20	4·54	1·839	0·216	3·7
40:30:30	4·22	1·837	0·199	3·7
55:25:20	4·57	1·838	0·237	3·7
B. Two shells				
60:20:20	3·20	1·830	0·159	3·9
	1·19	1·923	0·031	
40:30:30	3·13	1·831	0·156	3·9
	1·06	1·923	0·121	
55:25:20	3·27	1·829	0·164	4·1
	1·22	1·924	0·119	

References

Azaroff L V 1963 *Rev. Mod. Phys.* **35** 1012
Azaroff L V 1977 *x-ray spectroscopy* (New York: McGraw-Hill)
Belli M, Scafali A, Bianconi A, Mobilio S, Palladino L, Reale A and Benattini E 1980 *Solid State Commun.* **35** 355
Best P E 1966 *J. Chem. Phys.* **44** 3248
Bianconi A, Incoccia L and Stipcich S 1983 EXAFS *and Near Edge Structure* (Berlin: Springer Verlag)
Dehmer J L 1972 *J. Chem. Phys.* **56** 4496
Eisenberger P and Kincaid B 1978 *Science* **200** 1441
Elliott S R 1984 *Physics of amorphous materials* (London: Longmans) p. 82
Grunes L A 1983 *Phys. Rev.* **B27** 2111
Hayes T M 1978 *J. Non-Cryst. Solids* **31** 57
Hayes T M and Boyce J B 1982 *Solid State Phys.* **37** 173
Hemlata S, Sarode P R and Rao K J 1983 *J. Non-Cryst. Solids* **54** 313
Lee P A, Citrin P, Eisenberger P and Kincaid B 1981 *Rev. Mod. Phys.* **53** 769
Lee P A, Teo B K and Simons A L 1977 *J. Am. Chem. Soc.* **99** 3836
Lytle F W 1965 in *Physics of non-crystalline solids* (ed.) J A Prins (Amsterdam: North-Holland) p. 12
Rao B G and Rao K J 1984 *Phys. Chem. Glasses* **25** 11
Rao K J and Wong J 1984 *J. Chem. Phys.* **81** 4832
Rao K J, Wong J and Weber M J 1983 *J. Chem. Phys.* **78** 6228
Rao K J, Wong J and Shafer M W 1984a *J. Solid State Chem.* **55** 110
Rao K J, Wong J and Rao B G 1984b *Phys. Chem. Glasses* **25** 57
Rao K J, Rao B G and Wong J 1985a (results to be published)
Rao K J, Rao B G and Wong J 1985b *J. Chem. Phys.* (communicated)
Rao K J, Wong J and Hemlata S 1985c *Proc. Indian Acad. Sci. (Chem. Sci.)* **94** 449
Parthasarathy R, Sarode P R, Rao K J and Rao C N R 1982 *Proc. Indian Natl. Sci. Acad.* **48** 119
Sayers D E, Stern E A and Lytle F W (1971) *Phys. Rev. Lett.* **27** 1204
Shulman R G, Yafet Y, Eisenberger P and Blumberg W E 1976 *Proc. Natl. Acad. Sci. USA* **73** 1384
Stern E A, Sayers D E and Lytle F W 1975 *Phys. Rev.* **B11** 4836
Stern E A 1978 *Contemp. Phys.* **19** 289
Stern E A 1981 in EXAFS *for inorganic systems, Proc. Daresbury Study Weekend* Compiled by C D Garner and S S Hasnain.
Teo B K and Joy D C 1981 EXAFS *spectroscopy techniques and applications* (New York: Plenum Press)
Teo B K and Lee P A 1979 *J. Am. Chem. Soc.* **101** 2815
Tsutsumi K, Aita and Ichikawa K 1977 *Phys. Rev.* **B15** 4638
Winick H and Donaich S 1980 *Synchrotron radiation research* (London: Plenum Press)
Wong J 1981 *Topics in applied physics, glassy metals I* (eds.) H J Gunderodt and H Beck (Berlin: Springer Verlag) Vol. 46
Wong J and Liberman H H 1984 *Phys. Rev.* **B29** 651